PERGAMON

Journal of Structural Geology 23 (2001) 1359–1372

JOURNAL OF STRUCTURAL GEOLOGY

www.elsevier.com/locate/jstrugeo

Deformation partitioning inside a fissure swarm of the northern Icelandic rift

O. Dauteuil[a,*], J. Angelier[b], F. Bergerat[b], S. Verrier[b], T. Villemin[c]

[a]*Geosciences Rennes, UMR–CNRS 6118, Campus Beaulieu, 35042 Rennes Cedex, France*
[b]*Laboratoire de Tectonique, ESA–CNRS 7072, UPMC, 4 place Jussieu, 75252 Paris Cedex 05, France*
[c]*Laboratoire de Géodynamique des Chaînes Alpines, UMR–CNRS 5025, Univ. de Savoie, 73376 Le Bourget du Lac Cedex, France*

Received 23 February 2000; revised 17 December 2000; accepted 19 December 2000

Abstract

Extension in an oceanic rift domain is accommodated by fissuring and faulting processes. The fissuring, including dike injection, involves extension and an increase in crustal volume, consistent with magma supply, as in oceanic ridge and hot spot contexts. The faulting mainly involves thinning and extension. The relationship between these two deformation modes is analysed in the northern rift of Iceland. In the active rift zone, deformation and volcanism occur within 2–3-km-wide fissure swarms separated by 10-km-wide zones where deformation is minor. Based on topographic and geological mapping, the local structure in a major fissure swarm was analysed. The fracture density increases near the faults, but also beyond their tips. The geometrical analysis of structures revealed that for the last 10,000 years, block faulting and tilting accommodated about one half of the extension, the other half resulting from fissuring. This distribution shows that even in an active volcanic zone with widespread magmatism, the stretching resulting from normal shear can play an important role. As estimated from the ages of eroded surfaces and lava flows, the deformation rates range between 1.5 and 15 cm/year. These values are compared with other rates estimated for different time intervals in the same area.

1. Introduction

In oceanic rifts, tectonic and volcanic processes display important variations in both space and time. Within the inner rift of an oceanic ridge, there is a close interaction between tectonics, plutonism and volcanism that occur simultaneously. In the shoulder areas, the tectonic processes dominate because the off-axis volcanism is scarce and not directly related to rift extension (Batiza et al., 1990).

The results from the FAMOUS program showed that the inner active zone of an oceanic rift is formed by a central part where the volcanic activity prevails, surrounded by two elongated domains where tectonic activity dominates, especially fissuring (Ballard and Van Andel, 1977). Observations on the seafloor during submersible dives, such as in the AMAR rift (Stakes et al., 1984; Kappel and Ryan, 1987) or the East-Pacific Rise (Macdonald et al., 1996), as well as field surveys in the rift of Iceland (Gudmundsson, 1987a,b; Gudmundsson et al., 1992), revealed the presence of narrow fissure swarms separated by wide domains with minor deformation. This rather inhomogeneous distribution of the rift deformation can be regarded as a kind of structural partitioning. It was interpreted as a segmentation process occurring at different scales (Macdonald et al., 1988; Fox et al., 1991).

In a rift zone, the number and size of the fissure swarms clearly depend on the type of oceanic rift. In a typical undersea rift, a fissure swarm usually ranges from some hundreds of metres to a few kilometres in width. The usual length of the fissure swarm cannot be accurately determined because of the obvious limitations in submarine observation; however, the few data available indicate that this length may reach a few hundreds of meters. In more detail, the width of the fissure swarms observed in the slow-spreading rift systems ranges from 10 to 5000 m, whereas it may reach 10 km in the moderate to fast-spreading rift systems (Macdonald et al., 1996).

This lack of homogeneity in the distribution of the extensional deformation across an oceanic rift zone raises a major tectonic problem: how is the strain distributed in space and time inside the fissure swarms, and what is the nature of the deformation? In more detail, what is the relative importance of the increase in crustal volume related to magmatic supply on one hand and the stretching related to normal shear deformation on the other hand? An answer to these questions would help to constrain better the nature of the tectonic process contemporaneous with magma supply in oceanic rifts.

* Corresponding author.

0191-8141/01/$ - see front matter
PII: S0191-8141(01)00002-5

Three types of structures accommodate stretching: joints, fissures and normal faults, the latter often being related to tilted block systems. Although joints play an important role in the development and evolution of series of faulted-tilted blocks, especially where the amount of tilting becomes large enough to induce their reactivation as normal faults (Angelier and Colletta, 1983), their contribution to the total extension is generally small compared with that of other brittle structures. Furthermore, in areas of volcanic rocks, the amount of strain accommodated by tectonic jointing is almost impossible to estimate because of the importance of thermal contraction resulting from cooling. Cooling joints predate the joints of tectonic origin, partly inhibiting their development and influencing their orientation. The total amount of extension can be approximated by consideration of other brittle structures, such as normal faults, dikes, fissures and veins. Within submarine rift areas, the difficult survey conditions result in a major limitation when one attempts to quantify the amount of extension associated with the different structures of a fissure swarm. Cowie et al. (1993), however, have estimated that faulting accounts for 5–10% of the total deformation in the East-Pacific Rise. Similar results have been obtained in the Mid-Atlantic Ridge (Cowie et al., 1993). Such studies are scarce and the accuracy is poor, however, mainly because of the limited possibilities of undersea observation. Better accuracy can be obtained on land, based on extensive field surveys. De Chabalier and Avouac (1994) carried out a structural analysis in the Asal rift where the faulting accommodates 5–15% of the total extension.

Despite the limited number of data, all the results mentioned above concur to suggest that in an oceanic rift context, faulting plays a limited role (about 5–15% of the total extension), and hence that the largest contribution comes from fissuring and volume change related to magmatic supply. In such cases, the extension is focused in narrow deformed areas, with a typical width of a few kilometres. It should be noticed, however, that most observations have been made in narrow rift zones. The case of a wide oceanic rift zone, like the rift of northern Iceland, is certainly more complex. In counterpart, accurate observation can be carried out on land in the Icelandic rift, where most of the deformation and volcanism occurs inside sets of elongated fissure swarms. These parallel fissure swarms are several kilometres wide and trend NEE–SSW within a wide axial zone that trends N–S in northeastern Iceland (Saemundsson, 1979, 1986; Gudmundsson et al., 1992). The width of this axial zone reaches 50 km (Fig. 1).

In this paper, we aim to provide not only an estimate of the amount and rate of extension in a typical fissure swarm inside an oceanic rift zone, but also an evaluation of the deformation partitioning between faulting and fissuring. For this purpose, we consider one of the fissure swarms of the rift of northern Iceland, and we focus on the deformation that has occurred in the last 10,000 years, according to the age of the deformed lava flows and erosion surfaces. To be as complete as possible in this structural analysis, we took into account not only the faulting and fissuring but also the block tilting in our analysis, which has never been done in such a context. Two independent and complementary methods have been adopted. The first method involves strain analysis based on geometrical observations of faults and open fissures in the field. The second method consists of determining the stretching rate produced by block faulting and tilting related to normal displacement along curved faults. This tilting was quantified by using a numerical restoration of the topography, which was initially flat prior to deformation (i.e. the top of fluid basalt flows). Both these methods are needed in order to obtain a reliable estimate of the total deformation.

A direct output of this study is the determination of the average strain rate during the last 10,000 years, which can be compared with other determinations. At the scale of the entire rift of Iceland, the kinematic reconstruction provided an extension rate of 1.9 cm/year for periods longer than 1 Ma (De Mets et al., 1994). For very short time periods (7 years, from 1986 to 1992) higher values were obtained, up to 5 cm/year (Hofton and Foulger, 1996), which result from the inhomogeneity of deformation in space and time as a consequence of the elastic response to plate separation. These authors suggested that the difference between the long- and short-term strain rates results either from a stress redistribution after a recent tectono–volcanic event in a viscoelastic-layered model, or from continued opening of dikes at depth in an elastic half-space. In this respect, our analysis of the deformation that occurred during the last 10,000 years in a fissure swarm of the rift of northern Iceland provides a velocity estimate at an intermediate time scale, and hence provides some constraints about the mechanical behaviour of the lithosphere.

2. Geological setting of the study area

Numerous fissure swarms are present in the active rift zone of Iceland, where they are more or less arranged in ‘en échelon’ patterns (Fig. 1) These fissure swarms affect large domains of basaltic flows younger than 800,000 years. This ‘en échelon’ pattern results from the slight obliquity (about 10°) of the plate separation relative to the trend of the rift zone in northeastern Iceland. The spreading direction is N104°E (De Mets et al., 1994), whereas the rift zone trends N–S. Note that such an obliquity reaches 40° in the Reykjanes peninsula of southwestern Iceland.

The area that we studied in detail belongs to the Krafla fissure swarm of northeastern Iceland. It is located south of the Tjörnes Fracture Zone, a major dextral transform zone. In this area, the rift-spreading obliquity is the smallest (Fig. 1), so that the effect of the oblique rifting widening (Dauteuil and Brun, 1996) is reduced in comparison with other rift sections of Iceland. In the last 800,000 years, the deformation has occurred along five fissure swarms in this

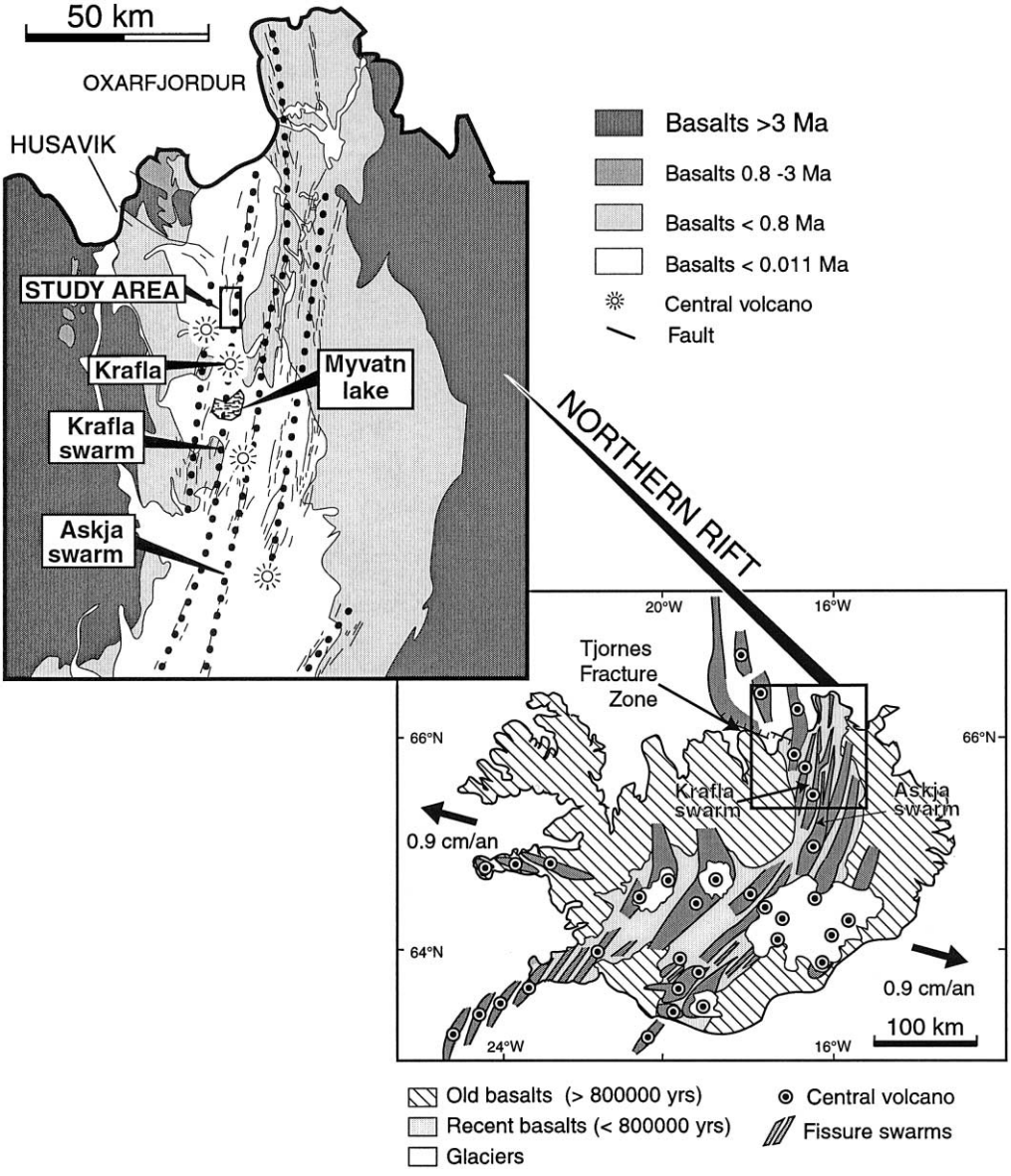

Fig. 1. Schematic map of Iceland showing the location of the fissure swarms. The 'en échelon' pattern arises from the obliquity of the spreading compared with the trend of the axial domain. The box indicates the study area (map from Saemundsson (1979, 1986)).

region, two of these swarms display very recent volcanism (less than 1100 years in age): the Krafla and the Askja fissure swarms (Fig. 1).

The Krafla fissure swarm is 80 km long, from south of Myvatn Lake to Axarfjordur Bay in the north, and 3–8 km wide. It cuts through the Krafla volcano characterised by an eroded caldera formed by dacitic welded-tuff (Björnsson et al., 1977). During Holocene times, at least 35 basaltic eruptions occurred just north of Myvatn Lake. The last two eruptions occurred in 1724–1729 and 1975–1984 (Björnsson et al., 1979) (Fig. 2). The age of the oldest lava flows is not accurately known, but they have undergone erosion during the last glaciation that ended 10,000 years ago, and hence are older than this elimatic event. The rift zone was the site of intense glacial erosion due to fast ice flow loaded by hyaloclastites erupted under the ice cap (Bourgeois et al., 1998). Therefore, the upper surface of the basalts eroded during the last glaciation constitutes an excellent marker, which is easily visible in the field and detectable in the SPOT satellite images. This eroded surface is thus used as a temporal reference to estimate the strain rate, and assumed to be 10,000 years old.

The survey area is located north of the 1975–1984 lava flows and west of the Möfell peak (Fig. 2). During the last seismic–volcanic episode, several earthquakes indicated shallow deformation due to magma intrusion into fissures (Einarsson and Bransdottir, 1980). Tryggvason (1984) measured a maximum widening of 8 m associated with the 1975–1981 rifting event, including the magmatic inflation; he estimated an average widening of 5–6 m

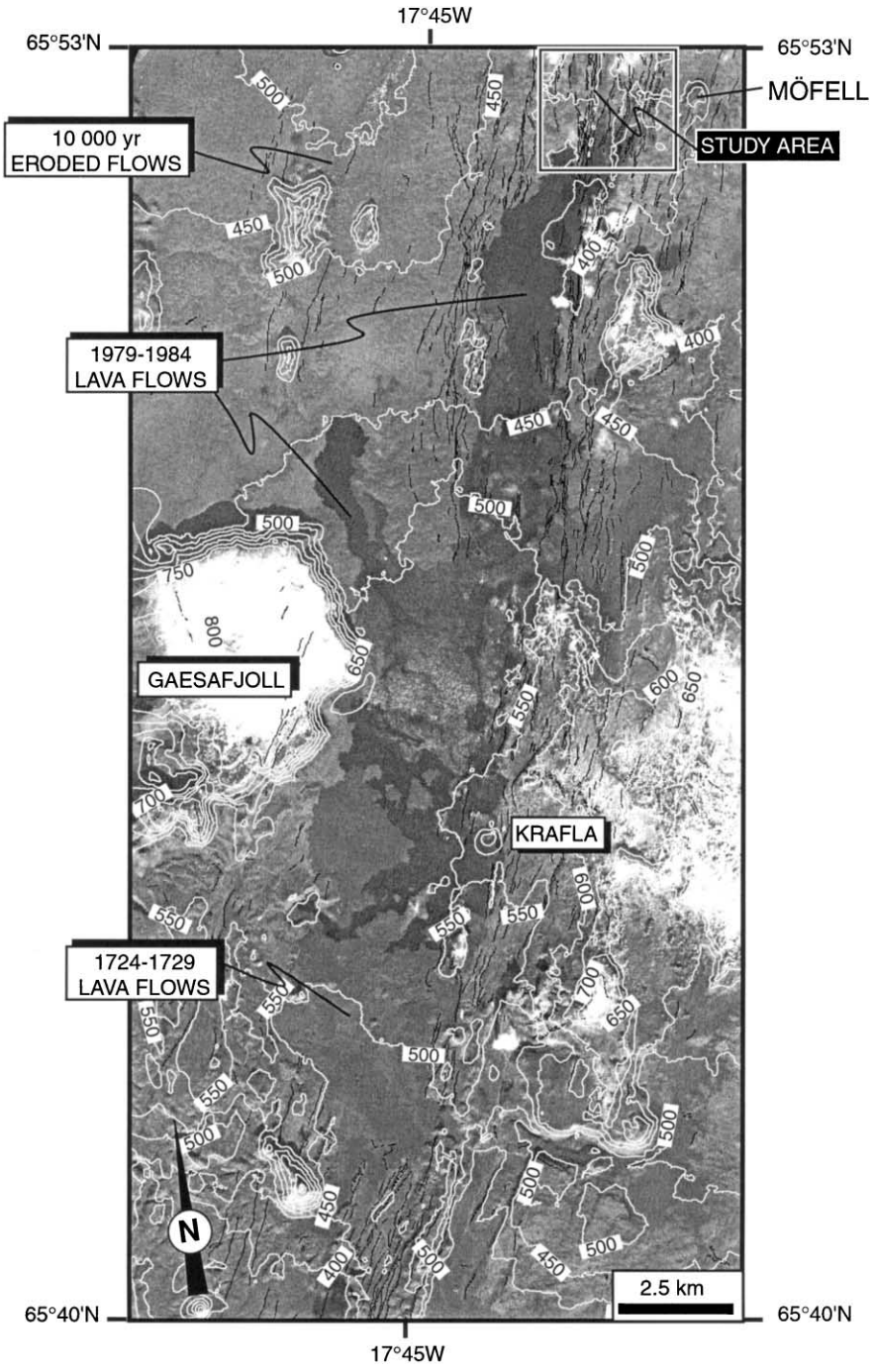

Fig. 2. SPOT image with elevation contours of the northern part of the Krafla fissure swarm. The thin black lines represent the fault and fissure patterns, the white lines are contours at intervals of 25 m, and the box at the top of the figure shows the area studied in detail.

along the 80 km of the Krafla fissure swarm. In terms of average extension rate, this value, estimated for a period of 6 years, reaches 1 m/year, i.e. nearly two orders of magnitude larger than the long-term velocity of divergence. Note that a recent satellite positioning (GPS) study indicated that this area was affected by a horizontal displacement of 5 cm/year during a period of 6 years (1987–1992), in the absence of any significant volcano–tectonic event (Hofton and Foulger, 1996). These discrepancies illustrate quite well the inhomogeneity of the extensional rates determined for very short time spans.

The most prominent feature in the structural scheme of the survey area is roughly the N015° graben. This graben acted as a channel for the lava flows during the latest 1975–1984 volcanic event (Fig. 2). To the south, this graben disappears while approaching the central caldera of the Krafla volcano, mainly because the successive lava flows filled up the tectonic depression (hiding its structure in this

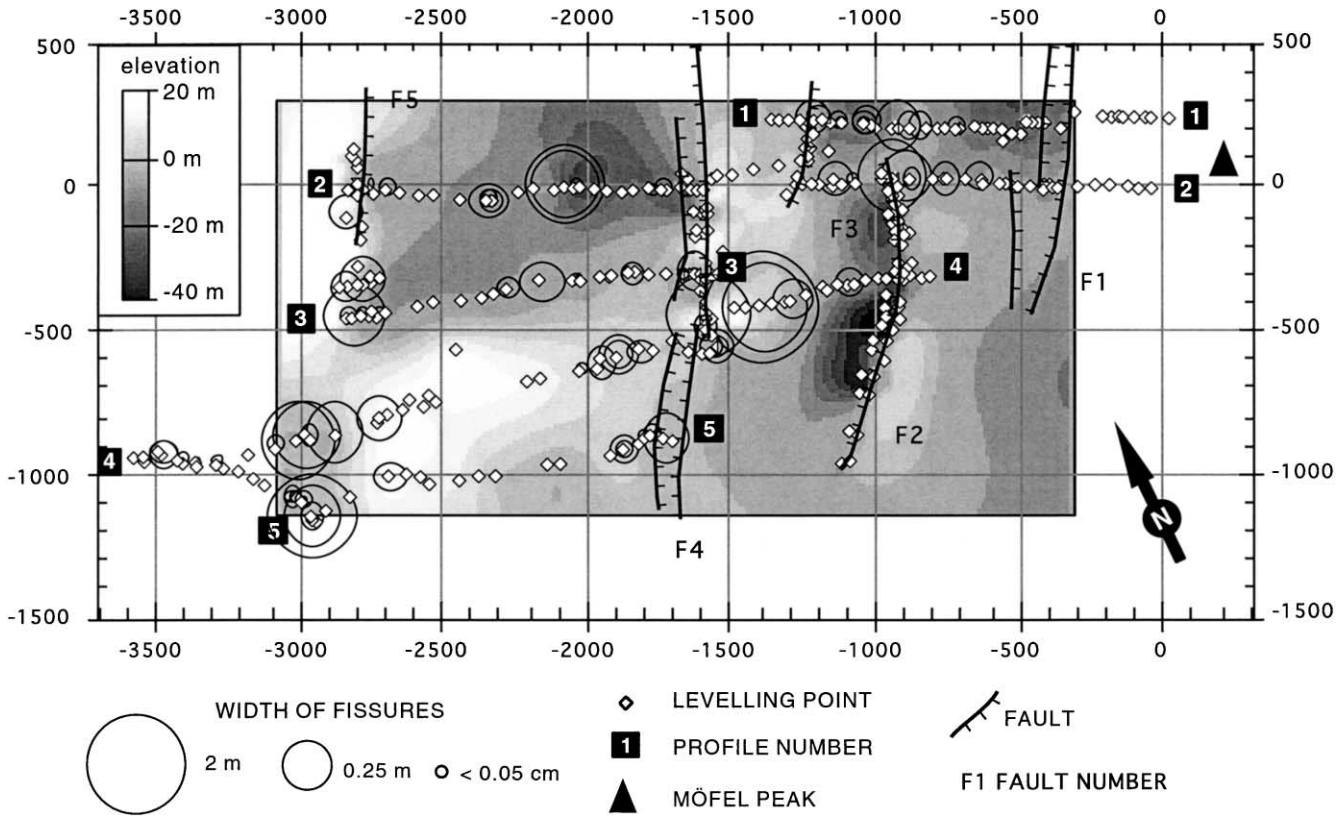

Fig. 3. Map showing the points measured in the Möfell area. The open lozenges indicate the point locations; the thick black lines the main faults with ticks oriented towards the down faulted block; and open circles are the fissures (the size of circle depends on the fissure width).

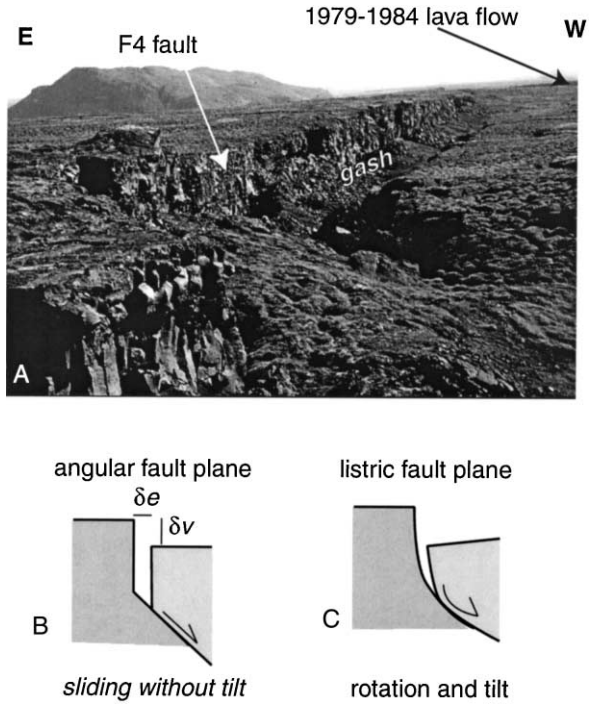

Fig. 4. The open fault of Icelandic fissure swarms. (A) Photograph of F4 fault; (B) section of open fault with an angular plane surface; (C) section of open fault with listric fault plane.

southern area). The width of this graben ranges between 2 and 3.5 km, and its maximum depth reaches 30 m. The fault pattern displays an azimuthal distribution with an average trend N010–020° (Opheim and Gudmundsson, 1989).

We principally considered the area located north of the 1975–1984-lava flow. The size of our detailed survey area is 3.2 km long in the E–W direction and 1.4 km long in the N–S direction (Fig. 3). Most structures were observed and measured along the profiles selected for topographic survey. For each feature (fault, fracture, etc.), the following data were recorded: location, strike, width and vertical offset. In order to quantify the deformation that had affected the initially flat surface, a topographic survey was indispensable. Therefore, we mapped the central active zone, more than 450 points being measured using a total station. Most of these points are distributed along five E–W profiles labelled 1–5 from N to S (see Fig. 3). Additional points have been measured along the main faults. The topography restoration involves a method that was especially set up for this work and will be presented in the corresponding section.

3. Structural analysis

Five main faulted zones, labelled F1–F5 from E to W affect this area (Figs. 3 and 4). They are formed by numerous faults trending from N005° to N030° (Fig. 5). The faults

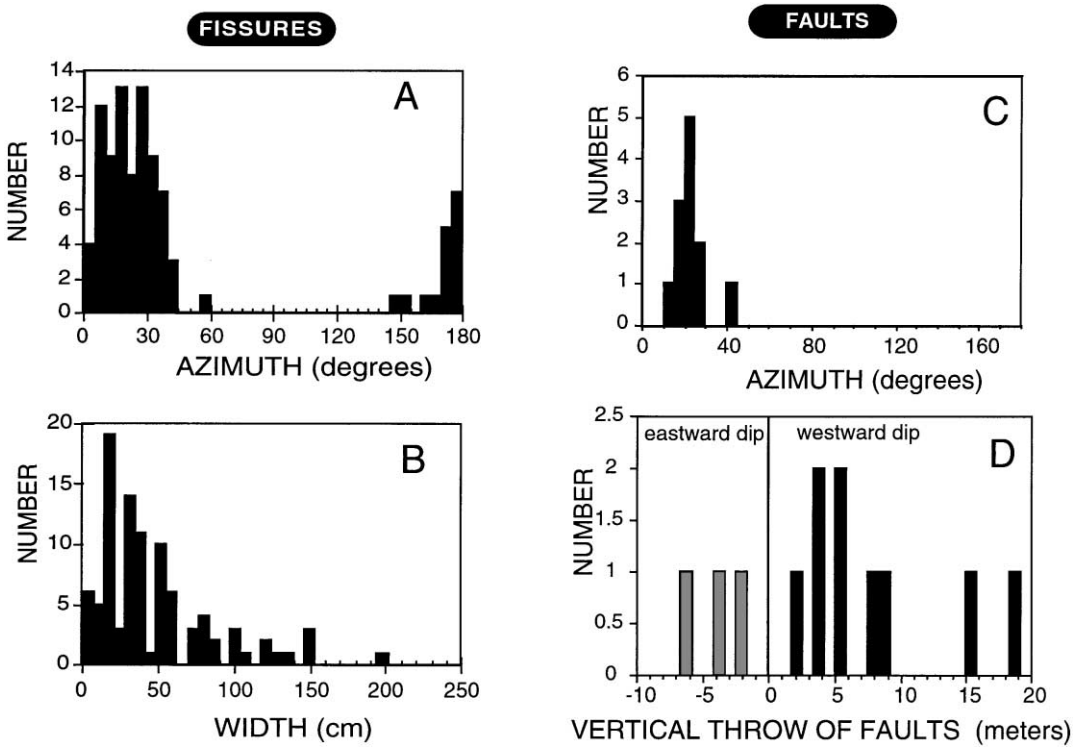

Fig. 5. Histograms of fissure azimuths (A), fissure width (B), fault azimuth (C) and fault throw (D). The locations of fissures and faults are indicated in Fig. 3.

display the classical aspect of the Icelandic-type open fault, previously described by Gudmundsson (1995) and by; Angelier et al. (1997). That is, the fault surface is nearly vertical and widely open. As demonstrated in the neighbouring Krafla area based on statistical measurements of the transverse horizontal opening and the vertical offset of such open faults, this aspect of active faults reveals that they are the surface expression of normal faults that have an average dip of about 60° at depth (Angelier et al., 1997). As a result, for such faults, the significant amount of opening associated with the vertical offset at the surface is expected to diminish and disappear at depth as the fault dip decreases (Fig. 4). It should be noted, however, that other fractures do not follow this geometrical rule and display a larger ratio between horizontal opening and vertical offset, revealing that at depth they may correspond to very flat faults or, much more likely, to dikes.

The largest vertical offset of fault measured in our study area reaches 18 m (Fig. 5d). For four of the main faults, the western side is down-faulted, consistent with a westward dip of the normal fault at depth. Along two of these major faults, conjugate systems of faults with smaller vertical offset (i.e. <5 m) are present. These systems contribute to form local small grabens, which are more or less tilted with the main blocks. The average trend of these faults is N025° (Fig. 5c).

A total of 93 fissures have been observed. Their trends range from N170° to N040°, with a peak value at N015° (Fig. 5a). Their width ranges from 10 cm to 2 m (Fig. 5b). The width distribution displays a maximum at 20 cm, followed by an exponential decrease in frequency towards high values of opening. The lack of small width values (i.e. <10 cm) has no mechanical significance, because it simply results from the observation conditions. At the surface, the moss and grass tend to effectively mask the smallest brittle features: a 25-cm-thick grass often hides the narrowest fissures. Most observed fissures are located close to the faults or between two closely spaced faults, the widest fissures being at the tip and in the prolongation of the main faults when disappearing. Between faults F4 and F5, a triangular area did not undergo fissuring; it is bounded to the west by a set of wide fissures and to the east by fault F4 (Fig. 3).

The different measurements collected are plotted along five profiles, labelled P1–P5 (Fig. 3). The distribution of the vertical throw along the faults indicates that the vertical motion is asymmetric, with downfaulting prevailing on the western side of the faults (Fig. 5d). Together with the topography of the top of the lava flow and the distribution of the fault offsets, this asymmetrical pattern is characteristic of block tilting. The amount of extension along each of these profiles has been computed using the following formula:

$$S = \Delta e/(L - \Delta e),$$

where L is the length of the profile, Δe the total dilation and S the stretching (Fig. 6; Table 1). The stretching ratios thus calculated range from 1.8×10^{-3} to 5.1×10^{-3}. This higher bound, found in Profile 4 only, strikingly differs from the other values and should be regarded anomalous. As their location in the map shows, Profiles 4 and 5 are particular because numerous large fissures, wider than 0.5 m, which

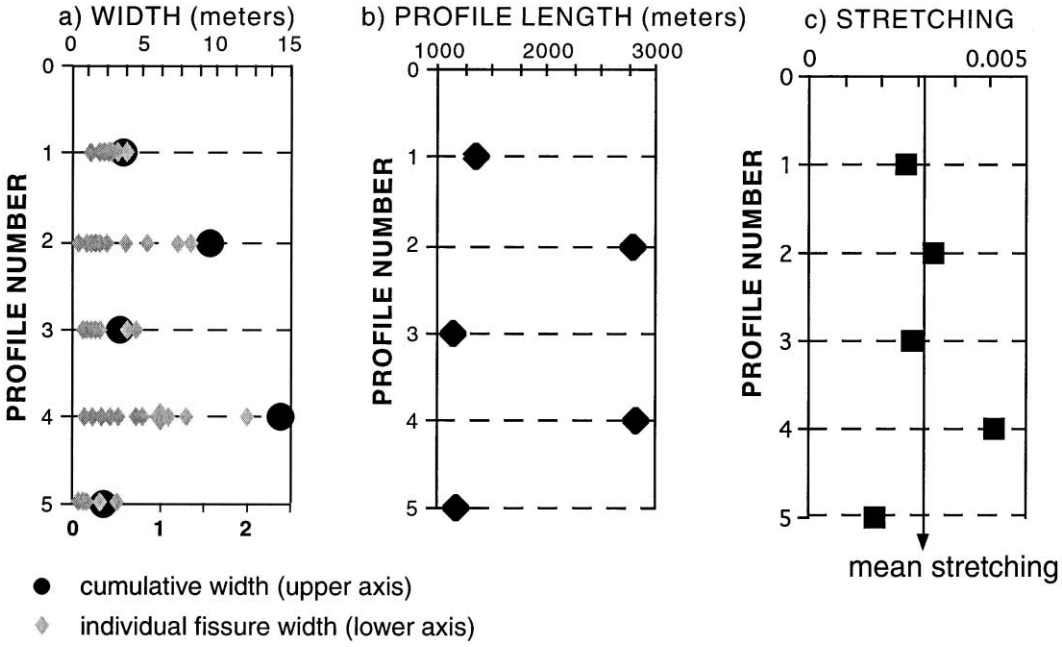

Fig. 6. Global analysis of deformation on each profile: (a) total dilation, (b) profile length, (c) stretching. The open circles correspond to individual measurements.

results in higher average stretching ratios, form the western boundary of the active zone. Without the value of Profile 4, the stretching ratio is quite homogeneous around 2.6×10^{-3}. It is important to note that despite this relative homogeneity in terms of stretching ratio, the raw dilation estimates display large variation (2.15–14.3 m).

Fault F5, located on the western side of the area studied, is the main fault of the graben. At the surface, it is nearly vertical. The dip at depth can be estimated using the method proposed by Angelier et al. (1997). The dip of the normal fault (α) is related to the total scarp height ($\Sigma\Delta_v$) and the total fissure dilation ($\Sigma\Delta_e$) by the following formula:

$$\tan\alpha = (\Sigma\Delta v)/(\Sigma\Delta e).$$

This analysis was applied to the western-central part of Profiles 2–5. In this area, analysis of the first three profiles reveal similar amounts of stretching (around 4×10^{-3}) (Table 2). However, the study along Profile 5 showed a low value (1.8×10^{-3}), indicating a smaller average dilation. According to the formula above, the fault dip (α) estimated at depth thus ranges from 43° (Profile 3) to 0° (Profile 5). The intriguing null value obtained in Profile 5 is in fact artificial: it simply results from the absence of faults along this profile (so that $\Sigma\Delta v = 0$). In other words, this anomalous 0° fault dip simply shows that in this profile the extensional deformation is accommodated by genuine open fissures (and dikes at depth), not by normal faults, the formula being invalid in this case. In a similar way, the calculated fault dip at depth is very shallow (11°) in Profile 4, because this profile is not bounded by a main fault to the west. This low theoretical value simply indicates that a large amount of extension corresponds to dilation across genuine tension fractures (fissures and dikes), not to normal shear at depth. This has strong implications for estimating the ratio between volume change (dilation and magma injection) and stretching (normal shear). In this respect, the comparison between vertical offsets and horizontal displacements deserves attention. Contrary to the case example analysed by Angelier et al. (1997) near the Krafla, where normal fault dips from 60 to 72° were obtained in agreement with other data from eroded rift areas of Iceland, the deformation in the Möfell area is characterised by low values, which involve a

Table 1
Deformation parameters measured or calculated on each profile of the whole studied area. $\Sigma\Delta e$: total dilation, L: length; S: stretching ($S = \Delta e/(L - \Delta e)$); $\Sigma\Delta v$ total vertical throw

Profile	$\Sigma\Delta e$	L	S	$\Sigma\Delta v$	$\Sigma\Delta v/\Sigma\Delta e$
1	3.58	1358.0	0.0026	1	0.27933
2	9.56	2790.0	0.0034	2	0.20921
3	3.30	1162.0	0.0028	− 4	− 1.2121
4	14.30	2814.4	0.0051	161	11.259
5	2.15	1178.0	0.0018	0	0.0000

Table 2
Deformation parametres measured and calculated on each of the central area. Deformation parameters measured or calculated on each profile of the whole studied area. $\Sigma\Delta e$: total dilation, L: length; S: stretching ($S = \Delta e/(L - \Delta e)$); $\Sigma\Delta v$: total vertical throw; x: dip angle of fault at depth

Profile	$\Sigma\Delta e$	S	$\Sigma\Delta v$	$\Sigma\Delta v/\Delta e$	α
2	5.48	0.004	4	0.72993	36.127
3	4.3	0.003	− 4	− 0.93023	42.930
4	9.6	0.004	2	0.20833	11.768
5	2.15	0.0018	0	0.0000	0.0000

significant component of dilation at depth rather than a very shallow dip of the normal faults. Thus, the shallow dips calculated by the formula above should be treated with caution, and one can infer that the fissuring related to magma injection at depth plays a significant role in the Möfell area.

4. Topography analysis

Part of the stretching is accommodated by slip along listric faults that tilt blocks. Such a tilted structure was described by Angelier et al. (1997) inside a small graben, south of the Krafla caldera. The amount of tilting is small (less than 5°) but can be accurately based on levelling measurements and topography restoration.

4.1. Method

The levelling data collection was performed by using a total station 'Topcon GTS 3B20'. The average accuracy is ±5 mm + 3 ppm for distances, and ±7 s for angles. The actual error in horizontal location (X,Y) was checked by measuring twice the relative position of a point at the beginning and the end of the survey: it is less than 20 mm. The error in elevation is less than 10 mm for the longest segment between the base points and the recorded point. The main source of uncertainty comes from the soil surface itself, however, which is very irregular because of the domes (thuffur) in the grass cover. Although we systematically recorded our points in a low position between the grass domes, the errors due to the grass remained high and may reach about 20 cm in elevation.

Eight base points have been used to survey the whole area with more than 400 points that are roughly placed in five W–E profiles and along the faults (Fig. 3). The first step was to gather all the levelling points into a single coordinate system attached to the first base station, located to the west of Möfell. To remove the rotation component between two bases, some external and distant landmarks (volcano summits) were systematically measured and used to calculate the parameters for the coordinate transform. Fig. 3 thus displays all the points in the same coordinate system.

A specific method for topographic restoration was developed to estimate the value and direction of block tilting resulting in vertical motion along the faults. Firstly, the study area was segmented into 11 elementary blocks whose boundaries correspond to a marked change in the topographic slope or to the presence of faults or large open fissures (Fig. 7). Considering the topographic data, the aerial photographs and the field structural observations performed this definition of 11 sub-areas. For the upper surface of each elementary block, a planar formulation constitutes a good geometrical approximation. The position (elevation, orientation and inclination) of the plane was through an inverse method using the least squares criterion, minimising the length between all the measured points (the data) and a theoretical plane (the unknowns). The most interesting final results are the dip value (D) and the dip azimuth. (Az) of each planar surface. The solutions for the 11 surfaces are given in Table 3, and are plotted in Fig. 7.

4.2. Results

According to these determinations, the tilts of the block range from 0.5° (sub-areas S01, S07, S10) to 3.1° (sub-area S11) (Table 3). The blocks S11 and S8 should be considered carefully because the inversion was poorly constrained (most data points being roughly aligned), and for this reason, these two results will be ignored in the discussion.

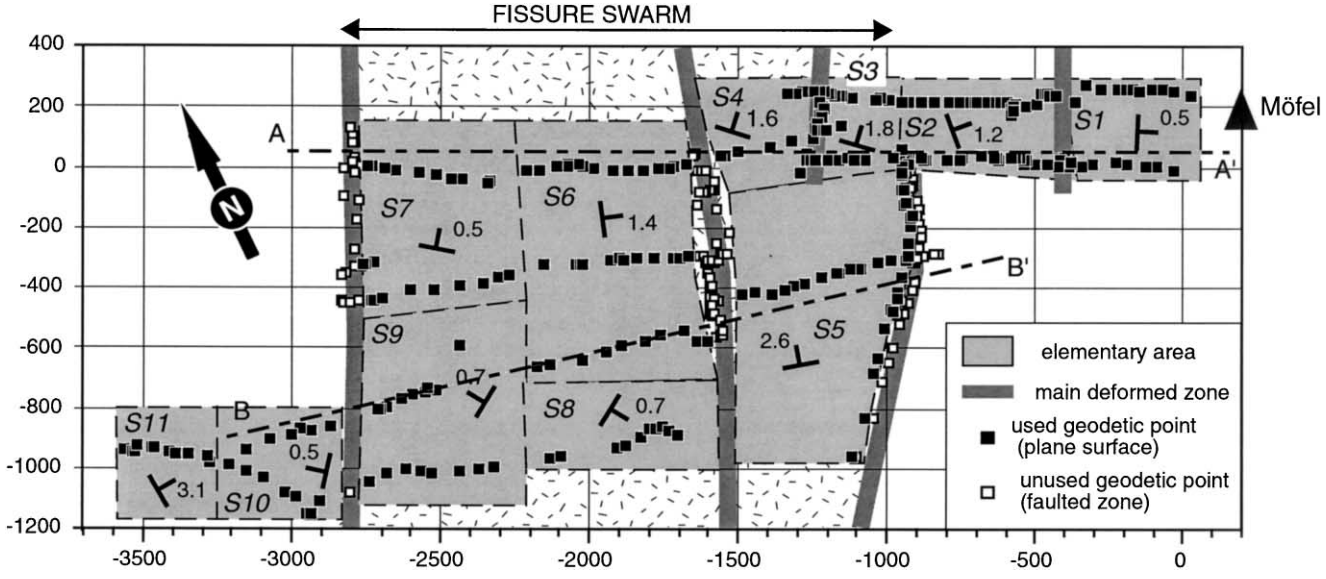

Fig. 7. Map of blocks isolated for the topographic analysis (dashed lines). Eleven blocks were delimited (S1–S11). The dip symbol indicates the mean slope trend of the block deduced from the best-fit plane calculation (see Table 3).

Table 3
Results of plane parametres calculation for the 11 elementary topographic surfaces. The parametres are given in Cartesian and spherical coordinates

	Dip azimuth	Dip angle	Plane formulation	Mean deviation of elevation
S01	92.6	0.5	$z = 0.00041$: $X = -0.00925$: $Y = -2.31852$	1.438
S02	69.6	1.2	$z = -0.00732$: $X = -0.01970$: $Y = -6.02965$	1.483
S03	27.1	1.8	$z = -0.02757$: $X = -0.01412$: $Y = -33.00637$	1.475
S04	16.6	1.6	$z = -0.2537$: $X = -0.00758$: $Y = -28.06231$	1.001
S05	−10.6	2.6	$z = 0.04519$: $X = +0.00848$: $Y = -50.5830$	1.997
S06	82.5	1.4	$z = -0.00327$: $X = -0.02473$: $Y = -13.03964$	1.604
S07	10.5	0.5	$z = -0.00897$: $X = -0.00171$: $Y = -24.01852$	1.658
S08	121.4	0.7	$z = 0.00632$: $X = -0.01034$: $Y = +7.05882$	0.620
S09	−58.0	0.7	$z = -0.00663$: $X = +0.01098$: $Y = +4.65823$	1.294
S10	−77.9	0.5	$z = -0.00188$: $X = +0.00880$: $Y = +4.95804$	0.968
S11	59.7	3.1	$z = -0.02734$: $X = -0.04688$: $Y = -192.000$	74.468

Typically, the blocks located on the eastern side of the deformed zone display the highest tilt angles. The lowest tilt angles were obtained in the outer sub-areas near the boundary of the fissure swarm. It is worth noting that, relative to the axis of the fissure swarm, the blocks are tilted outwards (except for S11). Note that the small dip values explain the wide range of dip directions to the E, N and W (but not to the S). Four blocks dip eastward or westward (that is, the dip direction is roughly parallel to the spreading direction), and three blocks dip towards the north.

From geometrical considerations of fault dip and azimuth, as well as from the analysis of elementary tilted surfaces, the lengthening due to faulting and block tilting can be estimated using the following formula (Fig. 8):

$$L - Lo = \delta Lr + \delta Lb,$$

where L represents the final length, Lo the initial length, δLr the lengthening resulting from block rotation along a curved plane, and δLb the lengthening due to the normal slip. A major simplification occurs because δLr can be considered negligible in our case as a result of the low values of tilt (less than 4°). Although the occurrence of block tilting in the

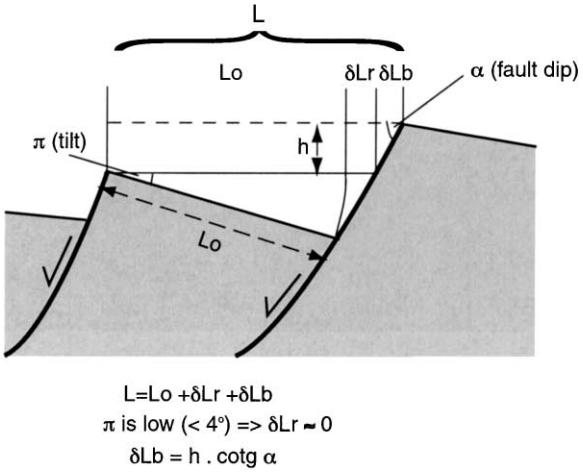

Fig. 8. Evaluation of the lengthening due to faulting and tilting. The final length (L) is equal to the initial length of the tilted block (Lo) plus the lengthening due to block rotation along a curve plane (δLr) plus the lengthening due to vertical throw along the faulted plane (δLb). δLr is assumed to equal zero because of the low value of tilt (<4°). Therefore, the lengthening due to one fault is given by $\delta Lb = h \cot g\ \alpha$, where h is the vertical offset and α the fault dip.

Table 4
Stretching balance between faulting and fissuring along two profiles (A–A′ and B–B′) located in Fig. 7. δLf: fissure lengthening, δLb: faulting lengthening, δLt: total lengthening, β: stretching ratio = $Lt/(Lt - \delta Lt)$

Profile	Length (m)	$\Sigma\delta L$f (m)	$\Sigma\delta L$b (m)	$\Sigma\delta L$t (m)	β	$\Sigma\delta L$f/$\Sigma\delta L$b
A–A′	2600	11.75 ± 5	13.10 ± 1	24.85 ± 6	1.0096 ± 0.001	0.908
B–B′	2500	11.86 ± 5	10.19 ± 1	22.05 ± 6	1.0089 ± 0.001	1.162

Möfell area plays an important role for constraining the structure of the blocks at depth (this paper), its influence for determining the amounts of extension remains negligible with respect to other sources of uncertainty. This situation contrasts with the case of most continental rifts where block tilting reaches large values and hence cannot be neglected in determinations of the extension amount (Angelier and Colletta, 1983). As a consequence of this simplification in the Möfell case study, a good approximation of the fault-related lengthening is obtained by simply considering the term $\delta Lb = h \cot g\ \alpha$, where h is the vertical offset and α the fault dip. In Iceland, an average dip of 67° for normal faults at moderate depths (1–2 km) is estimated from the studies of Gudmundsson and Bäckström (1991) and Angelier et al. (1997). In the Möfell area, the fault lengthening was estimated along two profiles: A–A′ and B–B′; The same value of 12 ± 5 m was obtained in both these cases (Table 4). The component of block tilting in the E or W directions is quite consistent with the direction of extension and rift opening; the block tilting in the northerly direction is not surprising because it occurs in a transition area and corresponds to local adjustment between two main normal faults.

5. Discussion

5.1. Structure of the fissure swarm

The Krafla fissure swarm to the north of the 1984 lava flow shows an asymmetric faulting pattern: a large single fault on the western side accommodates a vertical throw of about 40 m, whereas four fault sets are present on the eastern side. An area heterogeneously affected by fissures separates the western and eastern fault sets. The faults trend approximately N020° and generated eastward and westward tilts of the faulted blocks. The northward tilts are local, near fault tips or in transition areas between faults, that is at places where deformation involved a torsional component.

The western area of the swarm displays a particular deformation pattern (Fig. 3). The vertical offset of the westernmost fault (approximately 40 m to the north) significantly decreases to the south, so that the fault is finally replaced by a deformed zone affected by narrowly spaced wide open fissures located in a flexure zone with a clear topographic expression. East of this highly fissured fault-flexure zone, a large area where fissures are almost absent has been mapped. Therefore, three distinct domains can be distinguished within this fissure field (Fig. 9). In the first domain that surrounds the fault to the north, the fissuring mainly resulted from regional extension. The second domain is located on the convex part of the topographic flexure zone, so that most of the fissuring can be attributed to a back bending effect. In the third domain, concave flexing occurred and precluded fissuring and fracturing deformation inside the graben. This particular example illustrates well the structure of a transition zone between a normal fault and a flexure, and provides geometrical constraints concerning fault propagation.

5.2. Deformation partitioning

The two main methods used to decipher the brittle structure of the fissure swarm in this study enable us to better constrain the relative influences of dilation and magmatic injection inducing fissuring, and shear processes inducing thinning and normal faulting. In the South Leirnjukur graben, located near the Krafla volcano, most of the fissuring at the surface resulted from normal faulting, so that the influence of deep-seated dilation was minor and the influence of shear faulting could be analysed alone at the local scale (Angelier et al., 1997). In the larger Möfell area studied here, the volume change related to widespread fissuring is far from being negligible and thus deserves attention. This volume increase can be related to a magmatic phenomenon and/or tectonic dilation, that is magma injection beneath the fissure swarm studied. This balance was carried out along two synthetic profiles (A–A′ and B–B′) located in Fig. 7. The lengthening induced by fissuring is estimated in a simple way by summing the widths of all the nearly parallel fissures that crosscut each profile. The amounts of lengthening thus obtained are 22 and 25 m, giving a mean value of the stretching ratio of 1.009 ± 0.001 (Table 4).

Comparing the contributions of the fissuring and the faulting processes, it appears that each of these two processes accommodates about one half of the total strain (Table 4). A previous work carried out in the Asal rift led to a different ratio (De Chabalier and Avouac, 1994), with dike injection and fissure opening accounting for 90% of the deformation. Similar conclusions were obtained in the East-Pacific Rise (85–97%) and on Mid-Atlantic Ridge (80–89%) according to Cowie et al. (1993). Two explanations can account for the different proportion that we obtain. First, the importance of fissuring can be underestimated in our field analysis because moss and grass mask numerous

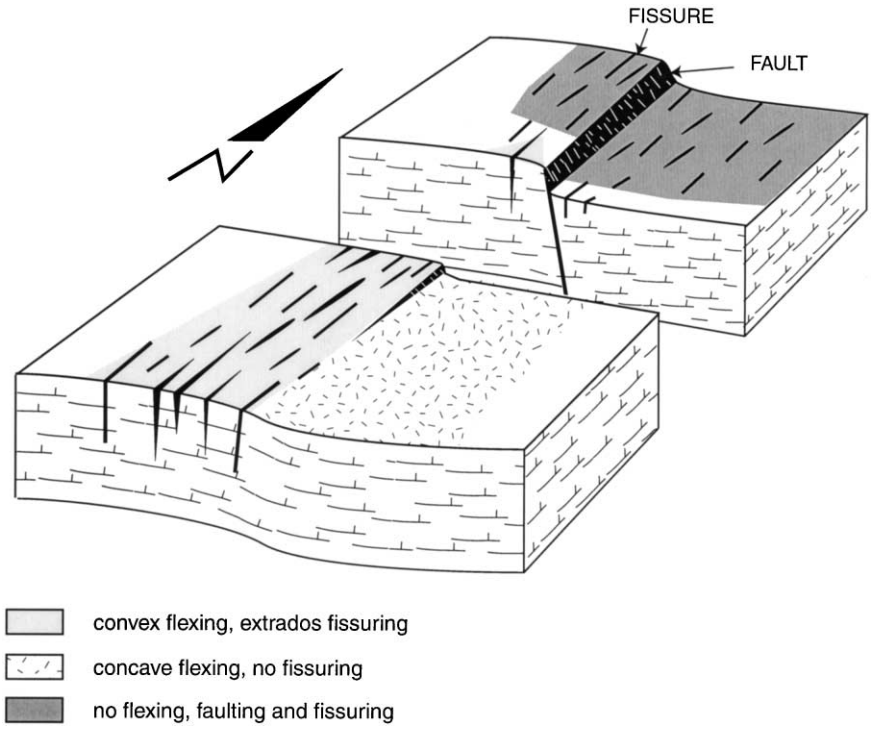

Fig. 9. Schematic 3D diagram of the western boundary of the Krafla fissure swarm where a fault evolves to a flexure. The fissuring results from the regional extension (dark grey area) close to the fault and from flexing (light grey area) on the top part of the southern flexure. The bottom part of the flexure is not affected by fissuring because it corresponds to a concave area submitted to compression.

small fissures. However, according to the exponential distribution of fissure frequency versus width, the total contribution of the smallest fissures is expected to be small compared with that of the other ones. We removed the grass and soil locally, and hence determined that the small fissures (with a width less than 10 cm) represent less than 15% of the observed set of fissures. This result in slightly underestimating the amount of fissure-related extension but has no potential to drastically change our result. The second explanation deals with the deformation style, especially the interaction between magmatism and tectonics where the faults should partly accommodate opening (Angelier et al., 1997). Where normal faulting occurs alone, the surface expression of normal faults includes a component of opening, which gradually diminishes at depth and finally vanishes in the absence of volume change. Where a genuine, deep-seated opening component generates a gash that allows upward migration of the magma and dike injection, this process often goes on with the fault sliding motion that thins the deformed volume, and which results in a combination of opening and shearing. At depth, the dip of such 'open faults' must be shallower than that predicted from the simple shear assumption. This hypothesis of normal faulting associated with opening at depth is not only supported by the very high ratio between openings and vertical offsets discussed before, but also accounts well for an intriguing aspect in the study area: the deficit in volcanism at the surface since 10,000 years ago, as compared with the large volumes expected according to the total dilation. Most of the magma migration has probably occurred at depth as it was the case, for instance, during the 1978 event (Einarsson and Bransdottir, 1980). That many dikes are present at shallow depths beneath grabens but fail to reach the surface as 'feeder dikes' and thus fail to produce volcanism has been pointed out and interpreted from the mechanical point of view by Gudmundsson (1990, 1995). Therefore, the upward migration of the magma is guided by open faults and fractures (dikes) above magma chambers where the magmatic fluid pressure is high. This upward migration becomes difficult at moderate depth, in the brittle layer of thinned upper crust where normal shear prevails while lithostatic pressure tends to close the conduits. This reason could explain why many dikes cannot reach the uppermost brittle layers where near-surface fissure opening prevails as the result of diminishing lithostatic pressure. This model with three layers is characterised by different relations between fluid pressures and lithostatic pressures (Fig. 10) and, hence, different ratios between dilation and simple shear (Angelier et al., 1997). It probably explains why we obtained such a high proportion of normal faulting-related extension in the upper brittle crust (the near-surface fissuring being left apart), compared with what should be expected according to the magma supply from the depth and, hence, the relative deficit in volcanism.

5.3. Time variation of strain rate

Based on our determinations, it is possible to estimate an

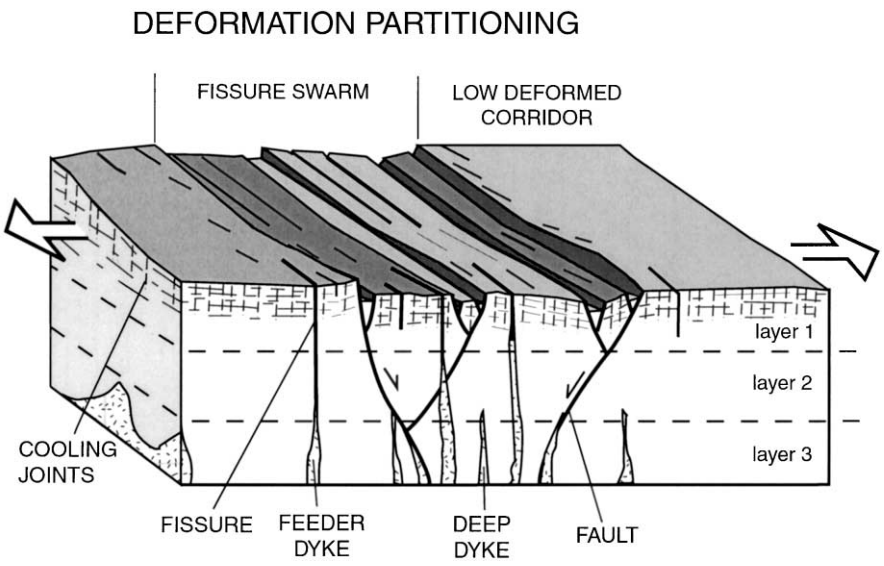

Fig. 10. Schematic block diagram of a deformation pattern in an extensional swarm (modified from Angelier et al. (1997)). The stretching is partitioned into joints (thin dashed lines), fissures (medium continuous lines) and faults (thick lines). The three layers discussed in the text are labelled: 1 (low lithostatic pressure), 2 (dominant normal shear and lithostatic pressure), and 3 (domain of high magma pressure). Level 2 represents a mechanical boundary to the upward migration of magma.

average strain rate by considering the age of the deformation. The described deformation affects the surface that was eroded during the last glaciation, giving a time interval. The Weichselian deglaciation occurred between 13,000 and 9,000 years ago, depending on the authors (Norddahl, 1990; Rundgren et al., 1997; Ingolfsson et al., 1997). In the present work, the deglaciation age is assumed to be 10,000 years. The Krafla fissure swarm has undergone a widening of around 1%, which corresponds to a mean value of 30 m considering the swarm width of 3 km. Since 10,000 years ago, this value implies an average rate of 3 mm/year. To evaluate the total amount of extension occurring inside the active zone, the values of the other fissure swarms must be integrated. In the rift of northern Iceland, the deformation is distributed into five fissures swarms (Fig. 1). Extrapolating the value obtained in the Krafla swarm to

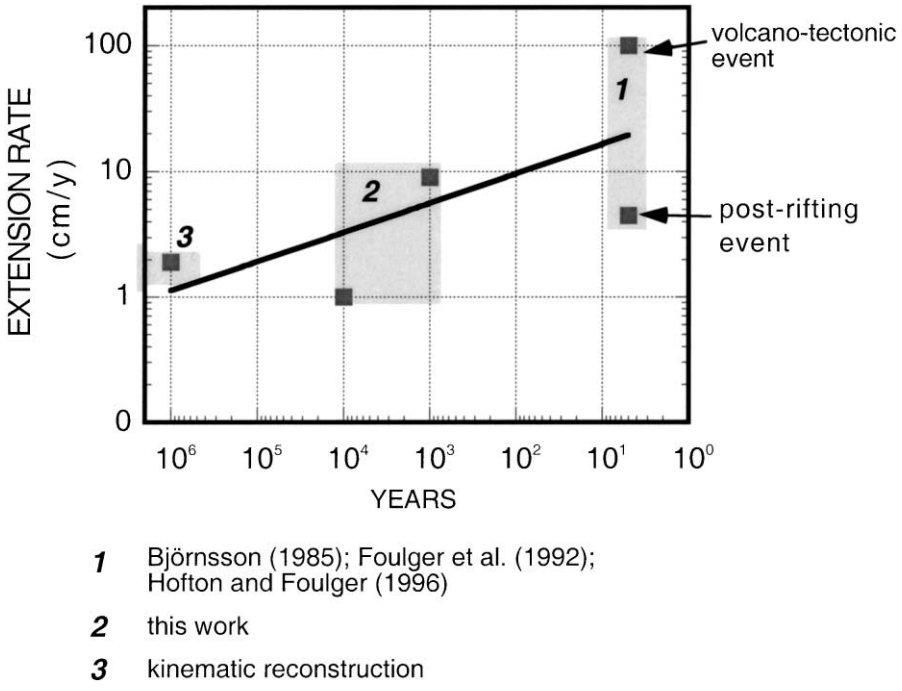

Fig. 11. Time evolution of the extensional rate through different time intervals of measurement: GPS methods (Tryggvason, 1984; Björnsson, 1985; Foulger et al., 1992; Hofton and Foulger, 1996) and kinematic reconstruction (De Mets et al., 1994).

the other swarms, one obtains an average extension rate of 1.5 cm/year for the entire rift zone, close to the value of 1.9 cm/year given by the kinematic reconstruction (De Mets et al., 1994). This rate is calculated by assuming that the deformation occurred since 10,000 years ago, and because the age adopted is a highest bound for the age of the deformation, the value of the strain rate that we obtain must be considered as a lower bound. As a lower bound for the age of the deformation, an age of 1000 years is considered because most of the deformation does not affect lava flows younger than 1000 years, as geological mapping indicates (Johannesson and Saedmundsson, 1998). We thus obtain the highest bound for the average rate of deformation, that is 15 cm/year for the entire active zone, more than seven times greater than the plate separation rate. Fig. 11 summarises the deformation rates estimated through different methods corresponding to various time scales. The higher rate is obtained during the instantaneous tectono–volcanic event, and can reach 1 m/year. Geodetic measurements by GPS that have been made in this area after a main rifting event, indicate a value of 5 cm/year (Foulger et al., 1992). Hofton and Foulger (1996a,b) interpret the high instant deformation rate occurring after a rifting event as due to a dike opening at depth in an elastic space. The stress redistribution in a viscoelastic half-space and in a viscoelastic layered medium does not fit with the data. At the local and regional scales, the deformation is a discontinuous phenomenon with cycles of intense activity (rifting events) separated by quiet periods. This aspect has been also described in the southern part of the Icelandic rift zone (Jonsson et al., 1997). Therefore, in Iceland, an average extension rate similar to this one estimated by integrating several millions years is obtained after 10,000 years. This value appears low taking into account the influence of the Holocene deglaciation, which generated additional deformation, and the co-seismic deformation, which cannot be estimated with the same methods. To go farther is this discussion it would be necessary to obtain data for a time span of 100,000–200,000 years (i.e. since the last interglacial period), which is still not the case.

The same discrepancy between short- and long-term deformation rates was also described in the Asal rift by Ruegg et al. (1990) and in the Aegean region (Jackson et al., 1994; Davies et al., 1997; Martinod et al., 1997). Several explanations can account for the recent high strain rate recorded during short periods: (1) a narrowing of the deformed zone (Ruegg et al., 1990; Bourgeois et al., 1998); (2) a stress release following its accumulation during a glaciation stage, (3) a change in plate boundary conditions or a particular tectono–volcanic event (Foulger et al., 1992; Hofton and Foulger, 1996); (4) a shift of the deformed zone (Helgason, 1984; Martinod et al., 1997); (5) a continuous dike injection at depth (Hofton and Foulger, 1996). This latter model seems unrealistic for long time period (greater than 1000 years), even if the strain rate can be high (greater than 5 cm/year) for relatively long time spans. To better constrain the complexity of the time evolution of the deformation, it will be necessary to record the deformation rates at different time scales and vital to better define the 3D geometry of the deformed zone.

6. Conclusion

In areas submitted simultaneously to extension and to volcanism such as oceanic rifts or hot spot rifts, fissuring and faulting accommodates the deformation. Previous studies indicate that the fissuring process dominates over faulting. Our work based on detailed structural mapping, gives an example where the roles of these two processes in the uppermost brittle layer are nearly equal for a period of 10,000 years. Two phenomena can be invoked to explain the high proportion of the faulting-related processes, as compared with determinations from other oceanic rift areas in the world: the volcanic activity was less intense in this part of the rift during the last period, or the tectonic activity was more intense because of the stress accumulation during the glaciation period. The deformation rate estimated for the entire rift zone since 10,000 years ago shows a wide range from 1.5 to 15 cm/year, suggesting that this time scale is scarcely sufficient to integrate the time variation of faulting and fissuring processes related to extensional tectonics and volcanism.

Acknowledgements

The help from the cooperation program French Ministère de Affaires Etrangères—Icelandic Ministry of Culture and Education and the French Embassy in Reykjavik is gratefully acknowledged. The CNRS–INSU projects Tectoscope and PNTS have supported this work.

References

Angelier, J., Colletta, B. 1983. Tension fractures and extensional tectonics. Nature 301, 49–51.

Angelier, J., Bergerat, F., Dauteuil, O., Villemin, T., 1997. Effective tension-shear relationships in extensional fissure swarms, axial rift zone of northeastern Iceland. Journal of Structural Geology 19, 673–685.

Ballard, R.D., Van Andel, T.H., 1977. Morphology and tectonics of the inner rift valley at 36°50′N on the Mid-Atlantic-ridge. Geological Society of American Bulletin 88, 507–530.

Batiza, R., Niu, Y., Zayac, W.C., 1990. Chemistry of seamounts near the East Pacific Rise: implications for the geometry of sub-axial mantle flow. Geology 18, 1122–1125.

Björnsson, A., 1985. Dynamics of crustol rifting in NE Iceland. Journal of Geophysical Reseach, 90 (B12), 10151–10162.

Björnsson, A., Saemundsson, K., Einarssan, P., Tryggvason, E., Grönvold, K., 1977. Current rifting episode in North Iceland. Nature 266, 318–323.

Björnsson, A., Johnsen, G., Sigurdsson, S., Thorbergsson, G., Tryggvason, E., 1979. Rifting of the plate boundary in North Iceland. Journal of Geophysical Research 84 (B6), 3029–3038.

Bourgeois, O., Dauteuil, O., Vliet-Lanoë, B.V., 1998. Pleistovene

subglacial volcanism in Iceland: tectonic implications. Earth Planetary Science Letter 164, 165–178.

Cowie, P.A., Scholz, C.H., Edwards, M., Malinverno, A., 1993. Fault strain and seismic coupling on Mid-Ocean ridges. Journal of Geophysical Research 98, 17911–17920.

Dauteuil, O., Brun, J.-P., 1996. Deformation partitioning in a slow-spreading ridge undergoing oblique extension (Mohns Ridge–Norwegian Sea). Tectonics 15, 870–884.

Davies, R., England, P., Parsons, B., Billiris, H., Paradissis, D., Veis, G., 1997. Geodetic strain of Greece in the interval 1892–1992. Journal of Geophysical Research 102 (B11), 24571–24588.

De Chabalier, J.-B., Avouac, J.-P., 1994. Kinematics of the Asal rift (Djibouti) determined from the deformation of Fieale volcano. Geology 265, 1677–1681.

De Mets, C., Gordon, R.G., Vogt, P., 1994. Location of the Africa–Australia–India Triple Junction and motion between the Australian and Indian plates: results from an aeromagnetic investigation of the Central Indian and Carsberg Ridges. Geophysical Journal International 119, 893–930.

Einarsson, P., Bransdottir, B., 1980. Seismological evidence for lateral magma intrusion during the July 1978 deflation of Krafla volcano in NE-Iceland. Journal of Geophysics 47, 160–165.

Foulger, G.R., Jahn, C.-H., Seeber, G., Einarsson, P., Julian, B.R., Heki, K., 1992. Post-rifting stress relaxation at divergent plate boundary in Northeast Iceland. Nature 358, 488–490.

Fox, P.J., Grindlay, N.R., MacDonald, K.C., 1991. The mid-Atlantic ridge (31°S–34°30′): temporal and spatial variations of accretionary processes. Marine Geophysical Research 13, 1–20.

Gudmundsson, A., 1987a. Tectonics od the Thingvellir fissure swam, SW Island. Journal of Structural Geology 9, 61–69.

Gudmundsson, A., 1987b. Geometry, formation and development of tectonic fractures on the Reykjanes Peninsula, southwest Iceland. Tectonophysics 139, 295–308.

Gudmundsson, A., 1990. Emplacement of dikes, sills and crustal magma chambers at divergent plate boundary. Tectonophysics 176, 257–275.

Gudmundsson, A. 1995. The geometry and growth of dykes. In: Heimann, Baer, G. and Heimann, A. (Ed.), Physics and Chemistry of Dykes. Rotterdam, Netherlands, pp. 23–44.

Gudmundsson, A., Bäckström, K., 1991. Structure and development of the Sveinagja graben, northeast Iceland. Tectonophysics 200, 111–125.

Gudmundsson, A., Bergerat, F., Angelier, J., Villemin, T., 1992. Extensional tectonics of southwest Iceland. Bulletin de la Société Geologique de France 163 (5), 561–570.

Helgason, J., 1984. Frequent shifts of the volcanic zone in Iceland. Geology 12, 212–216.

Hofton, M.A., Foulger, G.R., 1996a. Postrifting anelastic deformation around the spreading plate boundary, north Iceland, 1. Modeling of the 1987–1992 deformation field using a viscoelastic Earth structure. Journal of Geophysical Research 101 (B11), 25403–25421.

Hofton, M.A., Foulger, G.R., 1996b. Postrifting anelastic deformation around the spreading plate boundary, North Iceland 2. Implications of the model derived from 1987–1992 deformation field. Journal of Geophysical Research. 101 (B11), 25423–25436.

Ingolfsson, O., Björck, S., Halflidason, H., Rundgren, M., 1997. A review of the environmental history of Iceland, 13000–9000 yr BP. Journal Quaternary Sciences. 9, 147–150.

Jackson, J., Haines, J., Holt, W., 1994. A comparison of satellite laser ranging and seismicity data in the Aegean region. Geophysical Research Letter 21, 2849–2852.

Johannesson, H., Saedmundsson, K., 1998. Geological map of Iceland. Tectonics Icelandic Institute of Natural History, scale 1:500,000.

Jonsson, S., Einarsson, P., Sigmundsson, F., 1997. Extension across a divergent plate boundarthe Eastern volcanic Rift zone, south Iceland, 1967–1994, observed with GPS and electronic distance measurements. Journal of Geophysical Research 102 (B6), 11913–11929.

Kappel, E.S., Ryan, W.B.F., 1987. Volcanic episodicity and a non-steady state rift valley: evidence from SeaMark I observations. Journal of Geophysical Research 91, 13925–13940.

Macdonald, K.C., Fox, P.J., Perram, L.J., Eisen, M.F., Haymon, R.M., Miller, S.P., Carbotte, S.M., Cormier, M.-H., Shor, A.N., 1988. A new view of the mid-ocean ridge from the behaviour of the ridge-axis discontinuities. Nature 355, 217–225.

Macdonald, K.C., Fox, P.J., Alexander, R.T., Pockalny, R., Gente, P., 1996. Volcanic growth faults and the origin of Pacific abyssal hills. Nature 380, 125–129.

Martinod, J., Hatzfeld, D., Savvaidis, P., Katsambalos, K., 1997. Rapid N–S extension in the Mygdonian graben (Northern Greece). Geophysical Research Letter 24, 3293–3296.

Norddahl, H., 1990. Late Weichselain and Early Holocene deglaciation history of Iceland. Jökull 40, 27–50.

Opheim, J.A., Gudmundsson, A., 1989. Formation and geometry of fractures, and related volcanism of the Krafla fissure swarm, northeast Iceland. Geological Society of American Bulletin 101, 1608–1622.

Ruegg, J.-C., Gasse, F., Briole, P., 1990. Muvements du sol holocènes dans le rift d'Asal à Djibouti. Comptes Rendus de l'Académie des Sciences de Paris 310 (II), 1687–1694.

Rundgren, M., Ingolfsson, O., Björck, S., Jiang, H., Halflidason, H., 1997. Dynamic sea-level change during the last deglaciation of northern Iceland. Boreas 26, 201–215.

Saemundsson, K., 1979. Outline of the geology of Iceland. Jökull 29, 7–28.

Saemundsson, K. 1986. Subaeriel volcanism in the western North Atlantic. In: Vogt, P.R. and Tucholke, B.E. (Ed.), The Geology of North America. New York, pp. 69–86.

Stakes, D.S., Shervais, J.W., Hopson, C.A., 1984. The volcanic–tectonic cycle of the FAMOUS and AMAR valleys, Mid-Atlantic Ridge (36°47N): Evidence from basalt glass and phenocrist composition variations for a steady state magma chamber beneath the valley mid-sections, AMAR 3. Journal of Geophysical Research 89 (B8), 6995–7028.

Tryggvason, E., 1984. Widening of the Krafla fissure swarm during the 1975–1981 volcano–tectonic episode. Bulletin of Volcanology 47 (1), 47–67.